Biosensors and Bioelectronics 71 (2015) 294–299

Contents lists available at ScienceDirect

Biosensors and Bioelectronics

journal homepage: www.elsevier.com/locate/bios

Detection of Interferon gamma using graphene and aptamer based FET-like electrochemical biosensor

Sidra Farid [a,*], Xenia Meshik [b], Min Choi [a], Souvik Mukherjee [a], Yi Lan [a], Devanshi Parikh [b], Shripriya Poduri [a], Undarmaa Baterdene [b], Ching-En Huang [a], Yung Yu Wang [c], Peter Burke [d], Mitra Dutta [a,e], Michael A. Stroscio [a,b,e]

[a] Department of Electrical and Computer Engineering, University of Illinois, Chicago, IL 60607, USA
[b] Department of Bioengineering, University of Illinois, Chicago, IL 60607, USA
[c] Department of Chemical Engineering and Materials Science, University of California, Irvine, CA 92697, USA
[d] Department of Electrical Engineering and Computer Science, University of California, Irvine, CA 92697, USA
[e] Department of Physics, University of Illinois, Chicago, IL 60607, USA

ARTICLE INFO

Article history:
Received 19 February 2015
Received in revised form
15 April 2015
Accepted 17 April 2015
Available online 18 April 2015

Keywords:
Interferon-gamma
Graphene
Aptamer
Atomic Force Microscopy

ABSTRACT

One of the primary goals in the scientific community is the specific detection of proteins for the medical diagnostics and biomedical applications. Interferon-gamma (IFN-γ) is associated with the tuberculosis susceptibility, which is one of the major health problems globally. We have therefore developed a DNA aptamer-based electrochemical biosensor that is used for the detection of IFN-γ with high selectivity and sensitivity. A graphene monolayer-based FET-like structure is incorporated on a PDMS substrate with the IFN-γ aptamer attached to graphene. Addition of target molecule induces a change in the charge distribution in the electrolyte, resulting in increase in electron transfer efficiency that was actively sensed by monitoring the change in current from the device. Change in current appears to be highly sensitive to the IFN-γ concentrations ranging from nanomolar (nM) to micromolar (μM) range. The detection limit of our IFN-γ electrochemical biosensor is found to be 83 pM. Immobilization of aptamer on graphene surface is verified using unique structural approach by Atomic Force Microscopy. Such simple and sensitive electrochemical biosensor has potential applications in infectious disease monitoring, immunology and cancer research in the future.

1. Introduction

Tuberculosis is one of the major health problems globally and considered to be a lethal and common disease caused by *Mycobacterium tuberculosis* (Telenti et al., 1993). Research interest on this disease has increased exponentially since it is known to be one of the major death causes in HIV patients, affecting nearly 9.4 million patients and resulting in 1.7 million deaths worldwide (Castro and LoBue, 2011). Certain tests like *M. tuberculosis* direct test (MTD) and *Tuberculin* skin test (TST) has been performed conventionally in order to diagnose the tuberculosis infected patients, but such tests pose certain limitations, one of which is false positive results (Pfyffer et al., 1994). Some studies have shown that tuberculosis related cytokines can serve as biological markers for the active diagnosis of this disease (Walzl et al., 2011; Wallis et al., 2009). Cytokines are signaling proteins often secreted by a broad range of cells, including immune cells, in order to regulate the immune response, regeneration of tissues and wound healing process (Flesch and Kaufmann, 1993). One such cytokine is Interferon-gamma (IFN-γ) which is used to determine disease specific immune responses and can be used to serve as an active marker to diagnose infectious diseases like tuberculosis.

IFN-γ is an important inflammatory cytokine which is produced primarily by natural killer (NK) cells and thymus-derived (T) cells in response to various pathogens and possesses many physiological roles in immune systems and inflammatory stimuli (Seder et al., 1993). Detection of IFN-γ was tried traditionally with antibody-based immunosensing techniques which are sensitive and specific to cytokines, but these approaches are still hindered by the cumbersome, expensive and time consuming protocols employed (Luppa et al., 2001). In recent years, aptamers have emerged as a viable alternative to antibody-based immunoassays, offering the advantages of increased chemical/thermal stability, ease of modification and synthesis and higher resistance to denaturation under certain unfavorable conditions upon target binding (Zhao et al., 2012). These unique chemical characteristics

* Corresponding author.
E-mail address: sfarid3@uic.edu (S. Farid).

http://dx.doi.org/10.1016/j.bios.2015.04.047
0956-5663/

of single stranded DNA or RNA oligonucleotides called aptamers can be used for highly selective sensing of elements in various technological applications that utilize electronic, optical and piezoelectric readouts (Xu et al., 2014b; Farid et al., 2015, 2012).

With the increasing trend of aptamer-based studies, nucleic acid-based aptamers still remain a challenge and insufficiently explored until now. In this study, DNA-based aptamer is employed to be an active sensing element and IFN-γ is detected with high sensitivity on a conductive graphene-based platform. Graphene has a unique ambipolar characteristics and a large surface area that makes it a suitable candidate for biomolecular sensing (Li et al., 2009). In the past years, few studies have been reported showing graphene based field effect transistors (FET)-like structures using graphene oxide films as a sensing element to detect metal ions, etc. (Hu et al., 2013). Majority of the reports have been done using immobilization of DNA aptamers on a gold surface for the detection of the target molecules (Liu et al., 2010). Studies on using graphene-based field effect transistors (FET)-like structures that incorporate DNA aptamers as a molecular sensing element are still rare. In the past, our group has demonstrated successful detection of heavy metal ions like Pb^{2+} and K^{+} using graphene-based platforms (Xu et al. 2014a). In this work, we have successfully developed a nanosensor that is used for the detection of IFN-γ from the versatile graphene platform using aptamers as molecular sensing units and also employed a unique approach for immobilization of aptamer on graphene surface.

The sensing approach pursued in this work involves self-assembly of DNA based aptamer on graphene platform. Binding of IFN-γ molecules appears to change the charge distribution in the electrolyte, causing a current change across the highly conductive graphene. This change in current is detected and found to be dependent on concentrations of IFN-γ. Overall this electrochemical biosensor is found to be sensitive to IFN-γ and has potential applications in future.

2. Experimental

2.1. Fabrication of graphene based FET like structures

Liquid gate FET-like transistors were fabricated at University of California at Irvine by Wang et al. as described in their previous work in detail (Wang and Burke, 2013). Monolayer graphene is originally grown on Cu foil using low pressure chemical vapor deposition (LPCVD) process. Graphene was then transferred onto a polydimethylsiloxane (PDMS) substrate and Cu foil was etched away using 0.05 g/ml ammonium persulfate solution (Aldrich, > 98%). In order to verify if the graphene structure is established, Raman spectrum was taken using Reinshaw inVia Raman microscope with a 514 nm excitation input. Raman spectra was taken at multiple points using precise mapping and monolayer graphene peaks were detected. Structural analysis was done using SEM and AFM measurements in order to verify for any cracks on the graphene structure.

After the graphene layer is fabricated on PDMS substrates, another PDMS frame-like structure is attached onto the graphene platform in order to make a fillister that carries electrolyte for liquid gate probe, such that the monolayer graphene borders the bottom of fillister. After this PDMS well formation, FET-like structure is prepared by formation of source and drain electrodes on both ends of graphene layer using silver coating. The single graphene layer is used as a conducting substrate between the source and drain electrodes. The configuration of graphene-based biosensor is schematically shown in Fig. 1 (Fig. S1, Supplementary information). The conductance and functionality of graphene is tested using current–voltage measurements using an Agilent semiconductor parameter analyzer which will be explained in detail in the later section.

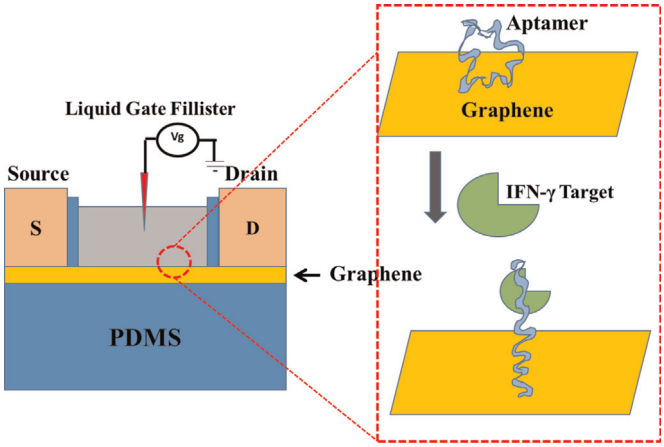

Fig. 1. Schematic of graphene-based electrochemical biosensor.

2.2. Immobilization of aptamers on graphene surface

IFN-γ aptamer with a 5′ pyrene modification (5′-/Pyrene/GGG GTT GGT TGT GTT GGG TGT TGT GT) was purchased from Biosearch Technologies, Inc. (Novato, CA) and dissolved in ultrapure Milli-Q water to form a stock concentration of 75 μM. A 10-μL drop of 75 μM aptamer in PBS was combined with 40 μL of anhydrous dimethylformamide (DMF) (Sigma Aldrich, St. Louis, MO), a commonly-used organic solvent, and the resulting 50 μL of 15 μM aptamer was then placed into the well of FET-like structure. All samples were left to incubate for 2 h at room temperature, after which they were washed three times in phosphate buffered saline (PBS) to remove unbound aptamers. After washing, the wells were filled with 50 μL of PBS. The detection of aptamer binding to graphene is proved further using Atomic Force Microscopy (AFM, Bruker ICON Dimension), in order to make sure that the aptamers are properly immobilized on the graphene surface. For control purposes, a second sample was prepared in the same manner as above, only using 10 μL of PBS (with no aptamer) and 40 μL DMF.

2.3. Electrochemical detection of IFN-γ

Recombinant human IFN-γ (R&D Systems, Minneapolis, MN) was dissolved in PBS and added to the well in increments to yield IFN-γ concentrations of 2 nM to 100 μM. Gate voltages of −0.8 V to +0.8 V were applied and the resulting source–drain current was measured for each IFN-γ concentration. Gate voltage was applied via a Ag/AgCl electrode with 1 mm tip (Microelectrodes, Inc., Bedford, NH), which was filled with 3 M KCl solution and placed in the well such that the tip was submerged in PBS but not touching the bottom of the well. Source and drain electrodes were placed on the silver-coated terminals. All *I–V* measurements were carried out on an Agilent semiconductor parameter analyzer at room temperature.

3. Results and discussions

3.1. Analytical selection of IFN-γ aptamer

The selection of DNA base sequence of IFN-γ aptamer was done analytically and chosen based on previously published studies as shown in Table 1 (Cao et al., 2014; Xiang and Lu, 2011; Tuleuova et al., 2010; Liu et al., 2010). While different groups have used

Table 1
List of IFN-γ aptamers used in previous studies.

No.	Sequence (5′–3′)	Ref.
1	CCGCCCAAATCCCTAAGAGAAGACTGTAATGACATCAAACCAGACACACTACACACGCA	Cao et al. (2014)
2	TGG GGT TGG TTG TGT TGG GTG TTG TGT	Xiang and Lu (2011)
3	GGG GTT GGT TGT GTT GGG TGT TGT GT (used in our experiment)	Tuleuova et al. (2010)
4	NH2-C6-GGGGTTGGTTGTGTTGGGTGTTGTGTCCAACCCCC3-SH	Liu et al. (2010)

somewhat different sequences for this aptamer, the sequence used by Tuleuova et al. (2010) (5′-GGG GTT GGT TGT GTT GGG TGT TGT GT-3′) seemed most suitable for our purposes for several reasons. This 26-base sequence is contained within the longer sequences used by Xiang and Lu (2011) and Liu et al. (2010), suggesting that it is the key motif for IFN-γ binding. Thus, the fact that at least three separate studies has demonstrated the effectiveness of this sequence led to its selection for use in this work. Another advantage of this sequence is its relatively shorter length, which makes it less likely to exceed the Debye length of the electrolyte. The electrolyte – in this case, PBS – contains an electrical double layer that screens the charges resulting from the binding of the target molecule to the aptamer (Maehashi et al., 2007). Any charges outside the Debye length are screened and their effects are not sensed by the graphene, so no current change would be detected regardless of target concentration. It is therefore important for the target-aptamer binding to occur within the Debye length, necessitating a short aptamer sequence.

The software Mfold was used to predict the most thermodynamically favorable conformations of the IFN-γ aptamer selected for this study (Fig. S2). The fact that there is minimal folding in all four conformations once again highlights the need for a short aptamer sequence that, even when fully extended, would not exceed the Debye length.

3.2. Structural verification of DNA-graphene binding using AFM

Instead of employing commonly adopted optical detection in order to verify binding of aptamer to graphene surface, which requires use of an aptamer with a fluorescent molecule attached, we have adopted rather simpler technique using Atomic Force Microscopy for DNA aptamer binding verification. Atomic Force Microscopy (AFM, Bruker ICON Dimension), was performed to make sure that the aptamers are properly immobilized on the graphene surface. For the first sample, 10 μL of 1 pM aptamer solution in milli-Q water was dropped on one side of graphene, and a small amount of DMF was also added to immobilize aptamers on the graphene surface before it was left overnight. The other side of the graphene was not exposed to the aptamer. After 12 h, both sides were washed thoroughly following the experiment protocol to remove unbound aptamers and any foreign substance, then excess water was removed by air. AFM measurements of 10 μm by 10 μm area including both the aptamer and the no-aptamer region along with height profiles of a part of regions is shown in Fig. 2. The color scheme was chosen to represent the difference more clearly. The aptamer region shows structures roughly a few hundred nanometers wide, and average of 30–50 nm tall, whereas the no-aptamer region does not have a distinguishable structure except for a few nanometer tall ridges which might be coming from the uneven surface of the PDMS substrate. These tall structures are assumed to be piles of aptamers binding to the graphene layer which is also confirmed by looking into the height profiles of the dotted regions (Fig. 2).

In order to verify our results for repeatability, another sample (sample B), was prepared similar to sample A. For the second measurement, a graphene transistor was prepared by dividing the

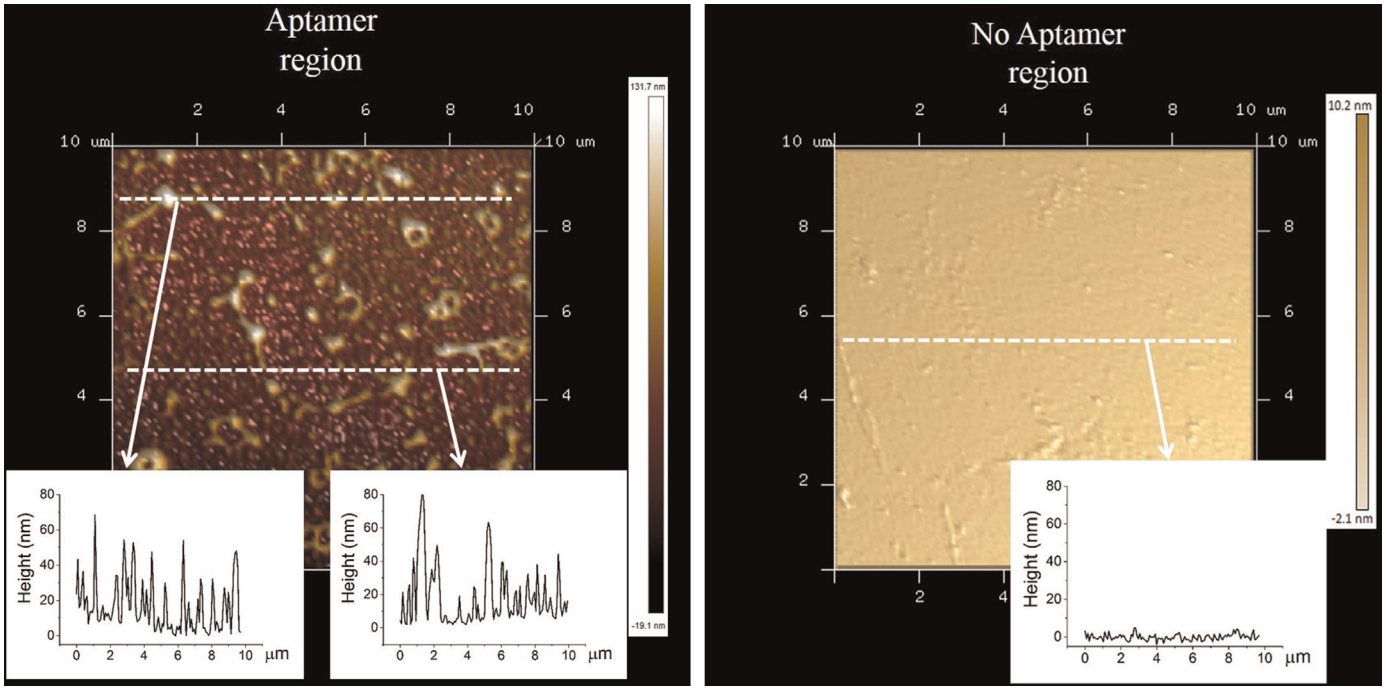

Fig. 2. Comparison between the aptamer and no-aptamer regions of sample A using AFM measurements of 10 μm by 10 μm area; subsets of plots indicate the height profile of parts of region shown by dashed lines. The aptamer region shows structures roughly a few hundred nanometers wide, and average of 30–50 nm tall, whereas the no-aptamer region does not have a distinguishable structure except for a few nanometer tall ridges which might be coming from the uneven surface of the PDMS substrate.

sample in half with an aluminum foil sheet. Similar aptamer solution in milli-Q water was dropped on one side of graphene, and was left overnight for water to be completely evaporated. Similar to the sample A result, the no-aptamer region only has ridges from the substrate (Fig. S3). The aptamer region has structures a few hundred nanometers wide, and an average of 50 nm tall whereas no aptamer region indicates 4–5 nm height profile. This clear contrast is also seen in sample A and the structures appears to be very similar to that, which clearly shows that aptamer successfully binds to graphene surface only and thus can be effectively used as a linker for the FET-like biosensor. Because of the destructive preparation procedure, these samples could not be used for the actual experiments.

3.3. Device characteristics

Conductivity and functionality of FET-like graphene-based devices is tested initially by adding PBS to the well. For checking the conductivity only between the source (S) and drain (D) terminals, I_{DS} versus V_{DS} curve is examined, which appears to be a straight line showing good conductivity of graphene between the two terminals of source and drain. The slope of this linear plot can also tell about the resistance between drain and source terminals. Wang et al. have shown that a typical resistance for a device with a 5 mm channel (as used in our study) is around 2.5 kΩ (Wang and Burke, 2013). This corresponds to a conductance of 400 μS. For checking the functionality of graphene and its ambipolar field effect semiconductor-like behavior, device transfer curve (drain current versus gate voltage) is taken, keeping the source–drain voltage (V_{DS}) constant at 0.3 V (Fig. S4). It is seen that the conductivity increases with the increase in gate voltage on both sides of the minimum conductance point. For the multiple device tested, minimum conductance point, also known as Dirac point, is found to be in the positive gate voltage range (0.1–0.5 V) depending on the doping state of each graphene film. In this paper, we have used change in current as a marker for detecting IFN-γ. The FET performance will allow us to monitor any change in current on addition of target molecules for sensitive detection of IFN-γ.

3.4. Graphene based electrochemical detection of IFN-γ

Device transfer curve is plotted after attaching aptamer to the graphene surface and adding concentrations of IFN-γ ranging from 0 nM to 100 μM while keeping V_{DS} constant at 0.3 V (Fig. 3A). It is noticed that as the concentration of IFN-γ is increased from 0 nM to 100 μM, a dynamic increase in current is observed in the n-conduction region of graphene which is the right side of the Dirac point, whereas decrease in current is seen in the p-conduction region (left side of Dirac point). It is also worth noticing that not only do we observe an increase in current at Dirac point, but also the Dirac point voltage appears to decrease and a negative shift in voltage is seen on increasing the target concentration (Fig. 3B). This shift in the Dirac point voltage could be the result of n-type doping effect due to introduction of charge carriers.

To understand more about the underlying mechanism of this graphene-based biosensor, we need to understand more about the device transfer curves of graphene-based FET devices. This transfer curve is divided into two separate branches along the two sides of the Dirac point. The type of conduction channel formed along either side of the Dirac point depends on the carrier density in the channel functionalized by the difference in voltage between the gate and the channel. Right side of the curve is known to form an n-type channel based on electron accumulation at higher gate voltages, whereas left side indicates p-type conduction channel with holes as majority carriers. The observed increase in current in n-conduction region and decrease in p-type channel is because as IFN-γ is introduced into the structure, it changes the electrical composition of the electrolyte (PBS). Because of the aptamer's short length, the target-aptamer binding occurs within the Debye length, so the resulting charges are not adequately screened by the ions in PBS and are thus “sensed” by the graphene. Electrons are donated to the graphene surface, which causes an increased carrier concentration resulting in enhanced current change in the channel. Similar observation is seen by Liu et al. (2010) who used DNA hairpin containing IFN-γ conjugated with methylene blue and also by Yan et al. (2013) who showed change in electron transfer efficiency. Thus our results revealed that graphene not only enhances electron transfer efficiency, but also can dynamically improve the signal efficiency and can also be employed as a signal amplifier.

3.5. Sensitivity and detection limit for IFN-γ sensor

The sensitivity and detection limit for our sensor is estimated at various IFN-γ concentrations. A nonlinear trendline based on Lorentzian model is fitted to the data points (I_{Dirac}) to estimate the sensor's sensitivity and to detect the upper bound above which the current saturates (Fig. 3B). The sensitivity of our device has been calculated by taking the first order derivative of the nonlinear regression equation. The sensor is found to be highly sensitive in the nanomolar range with an upper bound of ~10 μM above which the current saturates. In this work, the detection limit is

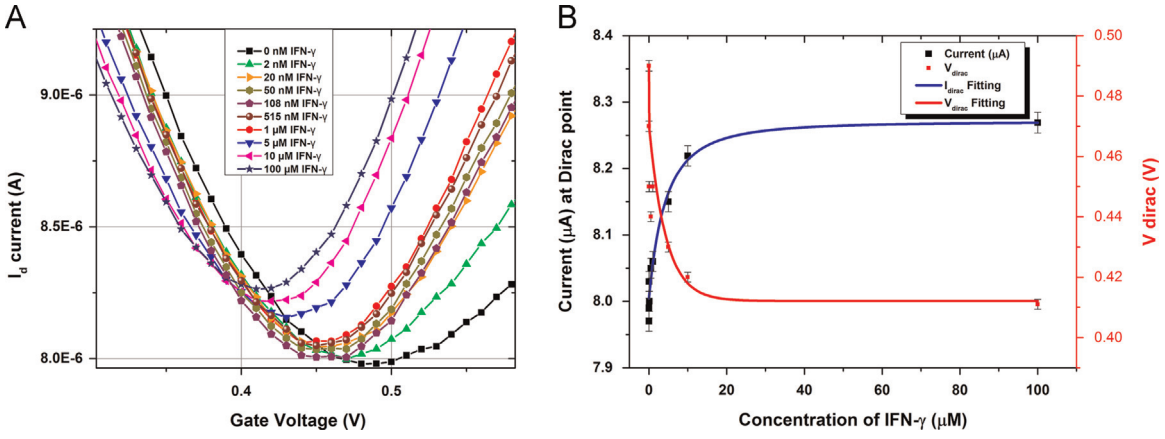

Fig. 3. (A) Device transfer curves for the FET-like structure after aptamer attachment and adding different concentrations of IFN-γ ranging from 0 nM to 100 μM; (B) response curves with Lorentzian and decaying exponential fit showing current and voltage at Dirac points respectively obtained at different concentrations of IFN-γ including error bars.

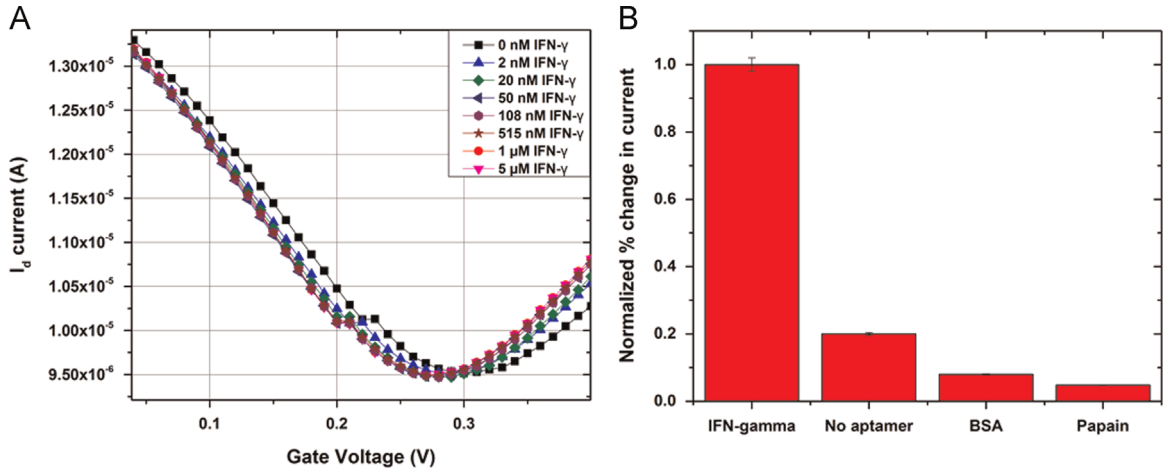

Fig. 4. (A) Device transfer curve for control experiments with no aptamer attached to graphene and IFN-γ concentrations ranging from 0 nM to 5 μM; (B) selectivity estimation by calculating normalized percentage change at dirac point at same concentration value (515 nM) for all target and non-target proteins including error bars. Normalization for all target and non-target protein is done with respect to IFN-γ target percentage change at 515 nM.

determined from the instrumental (HP 4155C parameter analyzer) resolution limit, which is 10 pA in the range of measurement of this work (Looke and Wentzell, 2012). Also, several assumptions are made for appropriate application of the technique. First, the sensitivity curve is assumed to obey log-normal distribution, which shows strong correlation (R^2=0.98) (Fig. S5). Second, the maximum sensitivity, which would give an even lower detection limit if it appeared lowered than the recorded, assumed to be equal to the highest in the data set. Lastly, the standard deviation of the blank measurement is assumed to be similar for each device. For the actual derivation, the measurement resolution limit is fitted into the sensitivity curve at which the product of the sensitivity and the concentration is equal to the measurement resolution limit. Our calculation show that, for the given instrumental limit, the lowest concentration is 82.7 pM. This detection limit is somewhat lower than Liu et al. (2010) and Tuleuova et al. (2010), and this simpler detection approach using a first-hand graphene based platform opens new opportunities for label free, simpler and amplified detection of other kinds of analytes as well.

3.6. Selectivity of IFN-γ sensor

Biosensors were investigated further using control experiments in order to verify their selectively and stability. For the control experiments, IFN-γ is introduced ranging from 0 nM to 5 μM concentrations in the pure graphene based FET-like structures without any aptamers. Device transfer characteristics are measured again keeping the drain voltage at the same value as previous sensor experiment (Fig. 4A). With the introduction of IFN-γ, no significant increase in current is observed whereas minimal change in Dirac point voltage is observed as compared to the sensor experiments on introduction of target molecules. To challenge our sensor more with nonspecific proteins, selectivity test was carried out using BSA and papain with the same concentration (515 nM) as well. As shown in Fig. 4B, the change in current in response to IFN-γ was much higher than for BSA and papain, and the control with no aptamer. This lack of response from the control experiments and significant increase in current from the functionalized sensor experiments reveals that the graphene-based biochemical sensor can be used for the active detection of IFN-γ with high sensitivity and stability.

4. Conclusions

We have successfully developed a graphene based FET-like bio sensor for detection of IFN-γ by taking advantage of dynamically high electron transfer efficiency of graphene platform. Binding of IFN-γ causes increase in electron current efficiency that provides a basis for detection. This enabled IFN-γ to be detected with a potential to reach target concentrations as low as 83 pM. To highlight biosensor selectivity, control experiments were performed and it is revealed that this biosensor is specific to IFN-γ target. A short DNA aptamer is chosen and DNA aptamer binding verification is achieved using AFM method instead of commonly-used optical detection.

A high-sensitivity biosensor for IFN-γ such as the one described in this work can be used in a variety of medical and biological applications. Blood and serum IFN-γ levels have been used to monitor the progression of diseases such as tuberculosis (Moura et al., 2004; Takenami et al., 2012) and malaria (Medina et al., 2011). IFN-γ levels of tuberculosis patients, for instance, have been shown to be around 1048 pg/mL before treatment and 2233 pg/mL after treatment (Moura et al., 2004). This change, equivalent to an increase of around 20 nM, can be easily detected with our sensor. Additionally, the fact that our sensor requires a very small sample volume (several μL) and gives an almost instantaneous result makes it convenient in medical settings. Compared to antibody based affinity biosensors, this graphene-based sensing platform provides advantage of not only chemical stability, but also the ability to be extended to other related targets. Because aptamers can be generated for such a wide variety of targets – ions, peptides, viruses, etc. – one would only need to change the aptamer while keeping the rest of the sensor identical in order to detect another analyte of interest. The proposed sensor therefore has a potential application in medical diagnostics, infectious disease monitoring and biomedical applications.

Acknowledgment

This work is supported, in part, by Army Research Office (ARO) through MURI Grant no. W911NF-11-1-0024.

Appendix A. Supplementary material

Supplementary data associated with this article can be found in the online version at http://dx.doi.org/10.1016/j.bios.2015.04.047.

References

Cao, B., Hu, Y., Duan, J., Ma, J., Xu, D., Yang, X.D., 2014. PLoS One 9, e98214.
Castro, K.G., LoBue, P., 2011. Emerg. Infect. Dis. 17, 337.
Farid, S., Mukherjee, S., Jung, H., Stroscio, M., Dutta, M., 2015. Mater. Res. Express 2, 025007.
Farid, S., Purahmad, M., Stroscio, M.A., Dutta, M, 2012. In: Proceedings of the 15th International Workshop on Computational Electronics (IWCE), IEEE, pp. 1–3.
Flesch, I.E., Kaufmann, S.H., 1993. Immunobiology 189, 316–339.
Hu, K., Liu, J., Chen, J., Huang, Y., Zhao, S., Tian, J., Zhang, G., 2013. Biosens. Bioelectron. 42, 598–602.
Li, X., Cai, W., An, J., Kim, S., Nah, J., Yang, D., Ruoff, R.S., 2009. Science 324, 1312–1314.
Liu, Y., Tuleouva, N., Ramanculov, E., Revzin, A., 2010. Anal. Chem. 82, 8131–8136.
Looke, H.P., Wentzell, P.D., 2012. Sens. Actuators B 173, 157–163.
Luppa, P.B., Sokoll, L.J., Chan, D.W., 2001. Clin. Chim. Acta 314, 1–26.
Maehashi, K., Katsura, T., Kerman, K., Takamura, Y., Matsumoto, K., Tamiya, E., 2007. Anal. Chem. 79, 782–787.
Medina, T.S., Costa, S.P.T., Oliveira, M.D., Ventura, A.M., Souza, J.M., Gomes, T.F., Vallinoto, A.C.R., Povoa, M.M., Silva, J.S., Cunha, M.G., 2011. Malar. J. 10, 1–10.
Moura, E.P., Toledo, V.P.C.P., Oliveira, M.H.P., Spindola-de-Miranda, S., Andrade, H. M., Guimaraes, T.M.P.D., 2004. Memórias Inst. Oswaldo Cruz 99, 283–287.
Pfyffer, G.E., Kissling, P., Wirth, R., Weber, R., 1994. J. Clin. Microbiol. 32, 918–923.
Seder, R.A., Gazzinelli, R., Sher, A., Paul, W.E., 1993. Proc. Natl. Acad. Sci. 90, 10188–10192.
Takenami, I., Finkmoore, B., Machado Jr., A., Emodi, K., Riley, L.W., Arruda, S., 2012. Pulm. Med. 2012, 1–6.
Telenti, A., Imboden, P., Marchesi, F., Matter, L., Schopfer, K., Bodmer, T., Cole, S., 1993. Lancet 341, 647–651.
Tuleuova, N., Jones, C.N., Yan, J., Ramanculov, E., Yokobayashi, Y., Revzin, A., 2010. Anal. Chem. 82, 1851–1857.
Wallis, R.S., Doherty, T.M., Onyebujoh, P., Vahedi, M., Laang, H., Olesen, O., Zumla, A., 2009. Lancet Infect. Dis. 9, 162–172.
Walzl, G., Ronacher, K., Hanekom, W., Scriba, T.J., Zumla, A., 2011. Nat. Rev. Immunol. 11, 343–354.
Wang, Y.Y., Burke, P.J., 2013. Appl. Phys. Lett. 103, 052103.
Xiang, Y., Lu, Y., 2011. Nat. Chem. 3, 697–703.
Xu, K., Meshik, X., Nichols, B.M., Zakar, E., Dutta, M., Stroscio, M.A., 2014a. Nanotechnology 25, 205501.
Xu, K., Purahmad, M., Brenneman, K., Meshik, X., Farid, S., Poduri, S., Pratap, P., Abel, J., Zhao, Y., Nicholas, B., Zakar, U., Stroscio, M., Dutta, M., 2014b. Design and Applications of Nanomaterials for Sensors. Springer, Netherlands, pp. 61–97.
Yan, G., Wang, Y., He, X., Wang, K., Liu, J., Du, Y., 2013. Biosens. Bioelectron. 44, 57–63.
Zhao, J., Chen, C., Zhang, L., Jiang, J., Yu, R., 2012. Biosens. Bioelectron. 36, 129–134.

Detection of Interferon Gamma using graphene and aptamer based FET-like electrochemical biosensor

Sidra Farid[a], Xenia Meshik[b], Min Choi[a], Souvik Mukherjee[a], Yi Lan[a], Devanshi Parikh[b], Shripriya Poduri[a], Undarmaa Baterdene[b], Ching-En Huang[b], Yung Yu Wang[c], Peter Burke[d], Mitra Dutta[a,e] and Michael A Stroscio[a,b,e]

[a]Department of Electrical and Computer Engineering, University of Illinois, Chicago, IL 60607, USA
[b]Department of Bio Engineering, University of Illinois, Chicago, IL 60607, USA
[c]Department of Chemical Engineering and Materials Science, University of California, Irvine, California 92697, USA
[d]Department of Electrical Engineering and Computer Science, University of California, Irvine, California 92697, USA
[e]Department of Physics, University of Illinois, Chicago, IL 60607, USA

Supplementary Data

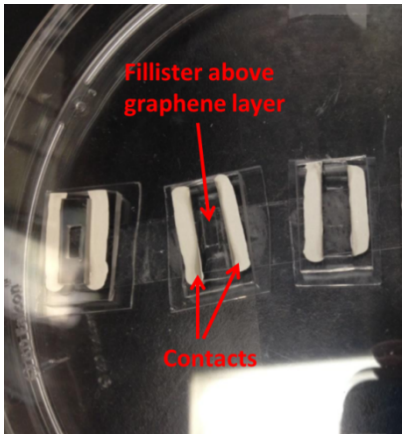

Fig. S1. Graphene-based electrochemical sensor platform.

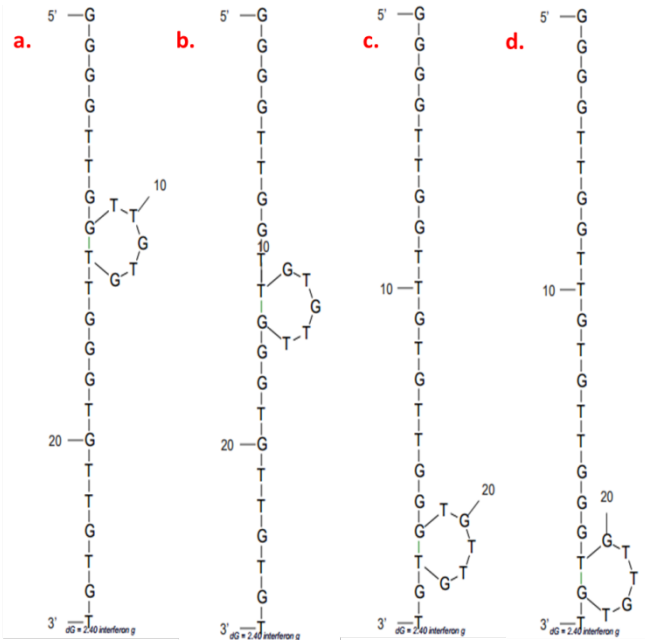

Fig. S2. Favorable conformations of the IFN-γ aptamer selected for this study using Mfold software (http://mfold.rna.albany.edu/?q=mfold).

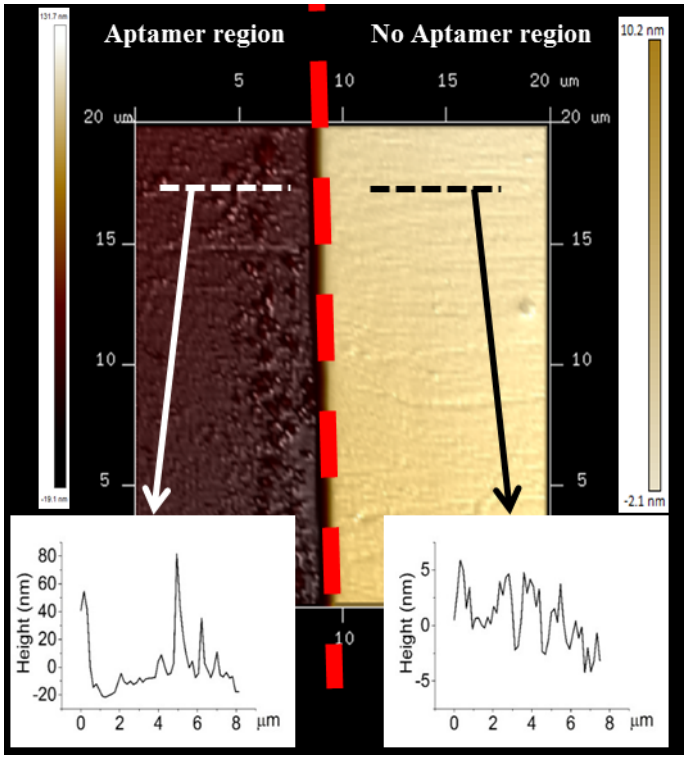

Fig. S3. Comparison between the aptamer and no-aptamer regions on sample B divided by an aluminum foil sheet along with height profile of parts of sample region indicated by dotted lines

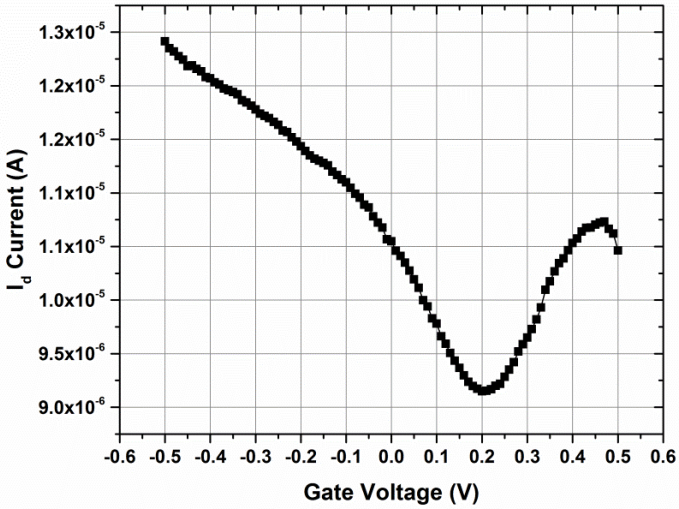

Fig. S4. Device transfer curve at constant source-drain voltage of 0.3 V.

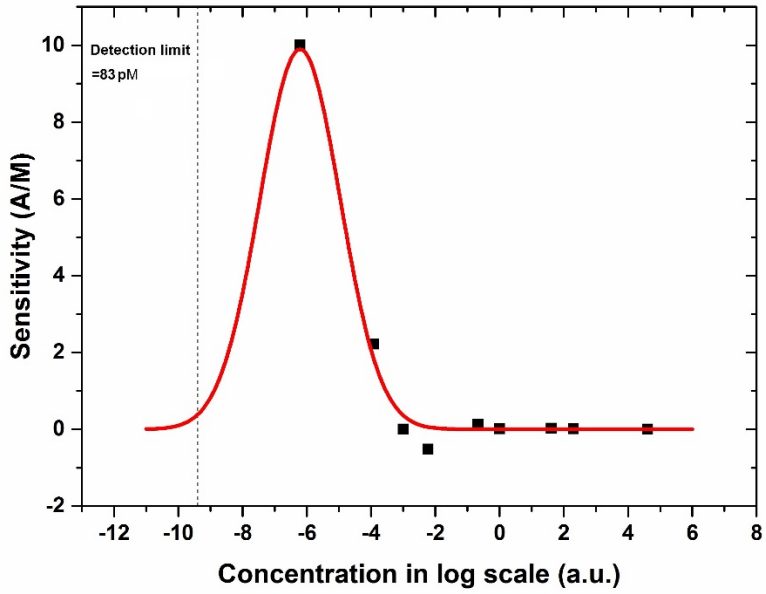

Fig. S5. Estimation of detection limit for our bio sensor for detection of interferon gamma. In this work, the detection limit is determined from the instrumental (HP 4155C parameter analyzer) resolution limit, which is 10 pA in the range of measurement of this work (Looke et al., 2012). For the actual derivation, the measurement resolution limit is fitted into the sensitivity curve at which the product of the sensitivity and the concentration is equal to the measurement resolution limit. Our calculation show that, for the given instrumental limit, the lowest concentration is 82.7 pM.